Materials Today • Volume xxx, Number xx • xxxx 2025 RESEARCH

ELSEVIER

RESEARCH: Original Research

Superior delamination resistant two-dimensional lamellar materials

Kaiwen Li [a], Lidan Wang [a], Feifan Chen [a], Jiahao Lu [a], Rui Guo [a], Yue Gao [a], Shiyu Luo [a], Xin Ming [a], Yue Lin [b,c,d], Zhen Xu [a,f,*], Manyi Huang [e], Chao Wang [e,*], Yingjun Liu [a], Chao Gao [a,f,*]

[a] MOE Key Laboratory of Macromolecular Synthesis and Functionalization, Department of Polymer Science and Engineering, Key Laboratory of Adsorption and Separation Materials & Technologies of Zhejiang Province, Zhejiang University, 38 Zheda Road, Hangzhou 310027, China
[b] CAS Key Laboratory of Design and Assembly of Functional Nanostructures, and State Key Laboratory of Structural Chemistry, Fuzhou 350002, China
[c] Fujian Science & Technology Innovation Laboratory for Optoelectronic Information of China, Fuzhou, Fujian 350108, China
[d] Fujian Institute of Research on the Structure of Matter, Chinese Academy of Sciences, Fuzhou 350002, China
[e] School of Astronautics, Harbin Institute of Technology, Harbin 150001, China
[f] Shanxi-Zheda Institute of Advanced Materials and Chemical Engineering, Taiyuan 030032, China

Numerous 2D sheets are generally exfoliated and prevalent to be assembled into macroscopic lamellar materials. However, these highly expected materials still inherit the easy exfoliation of 2D sheets and exhibit severe delamination failure problems, despite their outstanding in-plane performances and functions. Here, we find the increasing stack order of 2D sheets inversely aggravates delamination and uncover the hidden interlayer dissipation as the dominating mechanism. We propose a strong interlayer entanglement toughening strategy to greatly improve the delamination strength of graphene oxide papers by 268%, achieving a superior delamination resistance of benchmark natural nacres. The interlayer disentanglement offers extra dissipative sites to alleviate the stress concentration of the crack tip and suppress the crack propagation. This work provides an effective structural design strategy to resolve the intrinsic delamination problem of 2D lamellar materials, paving the way to realistic applications as structural materials and durable coatings.

Introduction

The easy exfoliation nature of mother lamellar crystals facilitates the birth of two-dimensional sheets but causes intrinsic delamination failure of their assembled lamellar materials [1–4]. In the surging research trend of 2D materials, laminated crystals with high in-plane but weak interlayer strength are usually exfoliated into individual sheets, exemplified by graphene [5,6], MoS_2 [7], BN [8] and MXene [9]. Diverse 2D sheets have been assembled into rich macroscopic materials, extending from papers [10,11], fibers [12–14] and coatings [15,16]. These macroscopic materials have exhibited outstanding mechanical and transport properties along the in-plane direction. The assembled papers of 2D sheets can have ultra-strength above 1 GPa and high stiffness up to 100 GPa [10,17–20], promising their use in realistic applications as structural components to withstand extreme mechanical loading. Despite the favorable in-plane properties, the neat macroscopic materials principally inherit the intrinsic conflict of the mother lamellar crystals and behave the easy failure trend with delamination [2,21–24]. This intrinsic delamination weakness greatly hampers the realistic applications to bear complicate deformations beyond simple in-plane tension.

* Corresponding authors at: MOE Key Laboratory of Macromolecular Synthesis and Functionalization, Department of Polymer Science and Engineering, Key Laboratory of Adsorption and Separation Materials & Technologies of Zhejiang Province, Zhejiang University, 38 Zheda Road, Hangzhou 310027, China (Z. Xu and C. Gao); School of Astronautics, Harbin Institute of Technology, Harbin 150001, China (C. Wang).
E-mail addresses: Xu, Z. (zhenxu@zju.edu.cn), Wang, C. (chaowang@hit.edu.cn), Gao, C. (chaogao@zju.edu.cn).

 https://doi.org/10.1016/j.mattod.2025.02.011

Please cite this article in press as: K. Li et al., Materials Today (2025), https://doi.org/10.1016/j.mattod.2025.02.011

Previous efforts have focused on promoting mechanical strength of assembled materials of 2D sheets, generally through enhancing the stack order or design the interlayer molecular interactions [10,11,17,19,20,25–27]. Increasing the stack order and density promoted the tensile strength of graphene assembled papers up to 1.1 GPa and the modulus to 60 GPa, through hydro-plastic stretching [10], high shearing coating [26] and water mediated pressing [27]. Design the interlayer interaction improved the strength of graphene paper to 1.8 and 98 GPa [19]. These efforts have pushed the in-plane mechanical limit of assembled materials, but ignored or even aggravated the easy delamination failure [4]. Some theoretical studies proposed a positive path to enhance the tensile strength of assembled materials by lattice disorder [28] and surface roughening [29] which decrease the regularity of stacking. Besides, improving the stress-transfer efficiency by stacking texture design is also a potential way to enhance interlayer adhesion and strengthen puncture resistance in out-of-plane [30]. To date, the systematic investigation of delamination failure of assembled 2D materials remains ignored and how to prevent the delamination is a challenge.

Here, we investigate the delamination behavior of the model graphene papers and reveal that the interlayer energy dissipation ability determines the delamination resistance, rather than the bonding strength. Inspired by the natural nacre, we propose an artificial interlayer entanglement toughening (IET) strategy to improve the interlayer energy dissipation, bringing the maximum 268 % and 328 % improvement in the delamination strength and the shearing strength in out-of-plane direction for graphene oxide papers. Strong interlayer entanglement introduced by ultra-high molecular weight polyvinyl alcohol (uPVA) enhanced the interlayer frictional resistance and dissipated substantial strain energy to suppress the initiation and growth of cracks, approaching the delamination resistance of benchmark nacre. The interlayer toughening strategy can be applied to design rich composites of other 2D materials with high delamination resistance, covering from reduced graphene (rGO), boron nitride (BN) and montmorillonite (MMT). Our work initiates resolve the intrinsic delamination conflict of assembled 2D materials and provides a general effective IET strategy to complement the long-ignored delamination deficiency, enabling realistic applications of prevalent 2D sheets.

Result

Intrinsic delamination behavior of 2D assembly materials

We firstly examined the delamination behavior of lamellar materials, including natural nacre and assembled papers of graphene. For natural nacre, we removed the interlayer organic glues by mild thermal treatment and the integrating bulk can be separated and peeled off to generate platelet debris (Fig. 1A, S1).

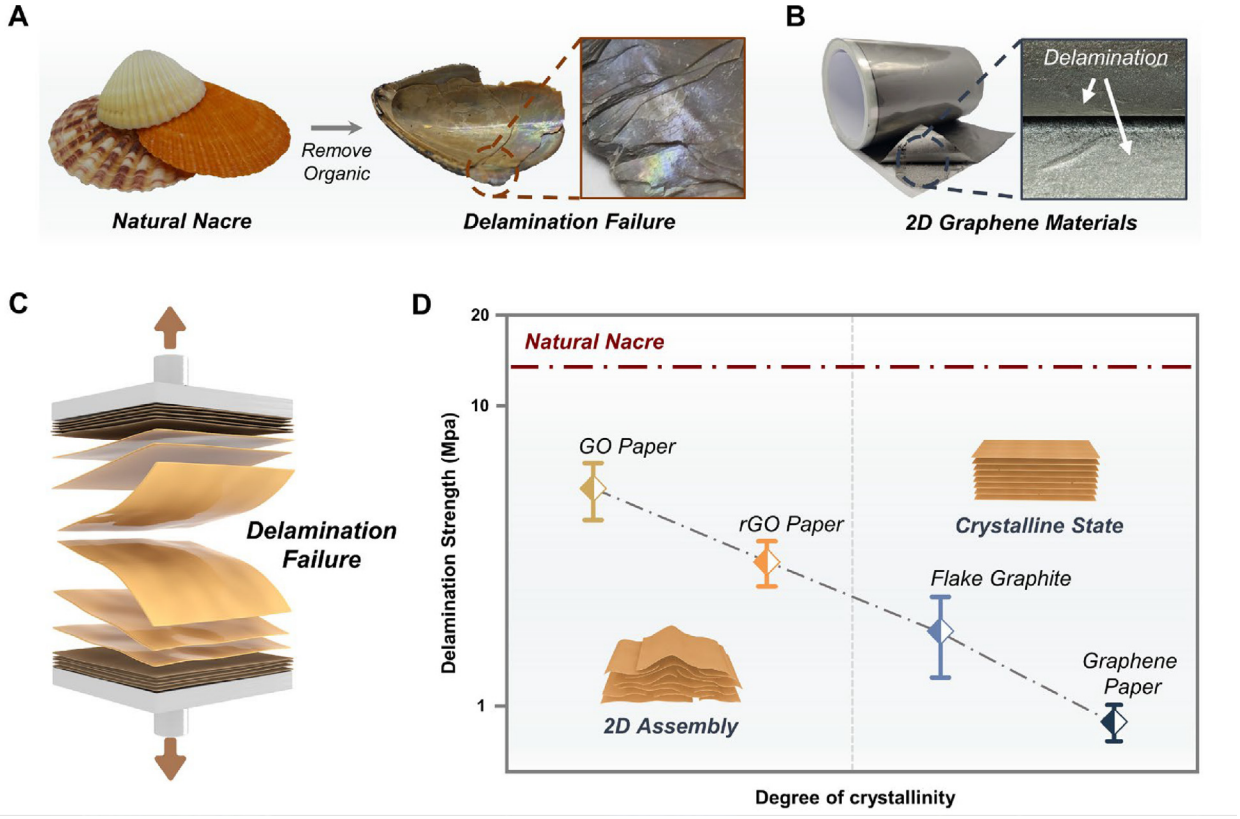

FIG. 1

Delamination failure behavior of 2D assembly materials. (**A**) Photographs of the delamination failure of the natural lamellar nacre when removing interlayer organic mortar. (**B**) Photographs of the delamination failure of the commercial graphene thermally conductive paper. (**C**) Schematic of the direct delamination test along out-of-plane direction. (**D**) Delamination strength versus crystallinity of four kinds of typical 2D graphene microscope materials and natural lamellar nacre.

Please cite this article in press as: K. Li et al., Materials Today (2025), https://doi.org/10.1016/j.mattod.2025.02.011

As to the assembled graphene paper, which is a commercial product for heat spreading, a severe delamination failure easily occurs, similar to the easy exfoliation of graphite (Fig. 1B, S2). In the direct delamination test, the interlayer binding strength is tested by perpendicularly pulling apart in the out-of-plane direction (Fig. 1C) to quantitatively evaluate the delamination resistance [31,32]. We examined the model graphene materials system extending from the well-known graphene oxide (GO) paper, reduced graphene oxide (rGO) paper and flake graphite and high temperature annealed graphene paper (Fig. S3). We found a strange trend that the delamination strength decreases as the increasing crystallinity, which principally means higher density, more regular stacking and stronger interlayer binding strength (Fig. 1D, S4). This counterintuitive trend denotes that the delamination is not directly determined by the interlayer binding strength.

In the comparable analysis of natural nacre, the interlayer protein glues bind rigid platelets and can provide excellent stress dissipation function of lamellar bulks [33–35], setting a benchmark delamination strength of 13.3 MPa (Fig. 2A, B). In graphene assembled materials, the enhancing interlayer stacking and binding have demonstrated a considerable promotion of in-plane strength and stiffness [10], however, brought delamination failure trend. In this case, we can conclude that the interlayer dissipation directly determines the delamination resistance of lamellar materials, but not pervious mere interlayer binding strength and stacking order [36–38].

In the theoretical fracture frame, the delamination can occur in two steps: the initiation of slit cracks and their propagation [39,40]. For highly crystalline graphite and mica, the delamination stress brings the burst of slit crack in the well-stacking structures (one is enough) and the propagation proceeds catastrophically along one slit crack plane to exhibit a smooth peeled surface [41], usually resulting in an atomically smooth substrate for atomic force microscopy (AFM) test (Fig. S5). As to the GO paper, the interlayer hydrogen bonds between GO sheets act as recoverable dissipating sites to resist the generation and propagation of slit cracks [42,43], resulting in a higher delamination strength (4.5 MPa) than that (3.4 MPa) of rGO paper even with stronger in-plane strength (Fig. 1D).

Artificial interfacial entanglement toughening design

Deducing the delamination failure mechanism, we proposed an artificial interlayer entanglement toughening (IET) strategy to enhance the delamination resistance of graphene assembled materials. We introduce ultra-high molecular weight polyvinyl alcohol (uPVA, $M_w = 1.2 \times 10^6$ Da) as the interlayer glue and the strong interlayer entanglement between uPVA chains and graphene sheets, providing efficient energy dissipation capability to resist delamination failure (Fig. 2C). Compared with the natural nacre, the introduced strong entanglement of uPVA chains dissipate the delamination energy by chain frictional sliding [18,44], acting as the fold-unfold cycling of interlayer proteins (Fig. 2A, S6). The softer GO sheets with better deformation ability and load transfer efficiency can also help to toughen assembled materials by allowing larger opening distance in delamination [2,40,45].

We used a tape peeling test to examine the delamination resistance qualitatively. Both nacre slice and uPVA-GO papers kept integrating after peeling by sandwiched copper tapes, exhibiting their excellent delamination resistance (Fig. 2B, D). By contrast, GO papers without uPVA can be easily peeled off (Fig. S7). To intuitionally assess the efficiency of strong entanglement, we used PVA with normal M_w (1.5×10^4 Da) as the interlayer binder and its GO composite paper was easily peeled into two layers (Fig. S8), similar to the delamination behavior of neat GO papers.

Fig. 2E shows the comparison of direct delamination strength curves of uPVA-GO papers, neat GO and normal PVA-GO papers. At the beginning, the lower slope of strength-displacement curve of the uPVA-GO paper implies the interior lower stress concentration to depress the generation of slit cracks, resulting from enhanced plastic deformation ability by introducing the uPVA which is a ductile phase and is primarily related to plasticity, that is, enlarging the plastic zone [40]. As delamination proceeds, the early inflection point in the uPVA-GO curve is attributed to that the highly entangled uPVA polymer is more fast responsive than the neat GO and normal PVA-GO to resist crack propagation with delamination deformation by the interlayer mechanical interlocking. Finally, uPVA-GO paper exhibits a larger delamination failure displacement (0.32 mm) than that (~0.2 mm) of neat GO and normal PVA-GO papers. Accompany with the larger displacement is the high ultimate delamination stress (11.8 MPa) of uPVA-GO paper, which is nearly two-folds higher than that of neat GO and normal PVA-GO papers. We also checked the peeling force with different loading angles by the 45°/90°/180° tape peeling tests, showing a collaborative contribution of highly entangled uPVA chains to improve both sheet deformation and interlayer delamination to relieve the delamination deficiency (Fig. S9). The remarkable improvement in delamination resistance by the proposed IET strategy demonstrates that the strong interlayer entanglement is effective for depress the occurrence of delamination at low polymer containing (Fig. 2F).

The delamination fracture also has an important effect on the overall mechanical performance with complex deformation manners, especially integrating with other components [46–48]. Aside from the direct delamination test, we conducted the lap-shear and stretching test to evaluate the delamination related performances (Fig. S10, S11). The lap-shear and tensile strength of uPVA-GO papers reach its maximum value of 18.4 MPa and 367 MPa respectively, showing a distinct increase than neat GO and normal PVA-GO papers (Fig. 2G, H). These indicate that the IET strategy is effective and powerful to improve the delamination resistance and relieve the intrinsic conflict in both directions for 2D lamellar materials.

Mechanism of interlayer entanglement toughening

We checked the microscopic mechanism of delamination of layered nacre, neat GO and uPVA-GO papers. The natural nacre exhibited a rough delamination failure section with sliding and crack deflection stages, which dissipate the energy to resist slit generation and propagation to enable its high delamination strength (Fig. S12) [33,49]. The neat GO paper showed smooth exfoliated fracture plane, which reflect the ease crack propagation to penetrate through one exfoliated plane (Fig. 3A, C). As to the uPVA-GO paper by the IET strategy (Fig. 3B, D), its delamination fracture surface has a quite rough morphology, which features with deflection stages and many dissipation structures,

Please cite this article in press as: K. Li et al., Materials Today (2025), https://doi.org/10.1016/j.mattod.2025.02.011

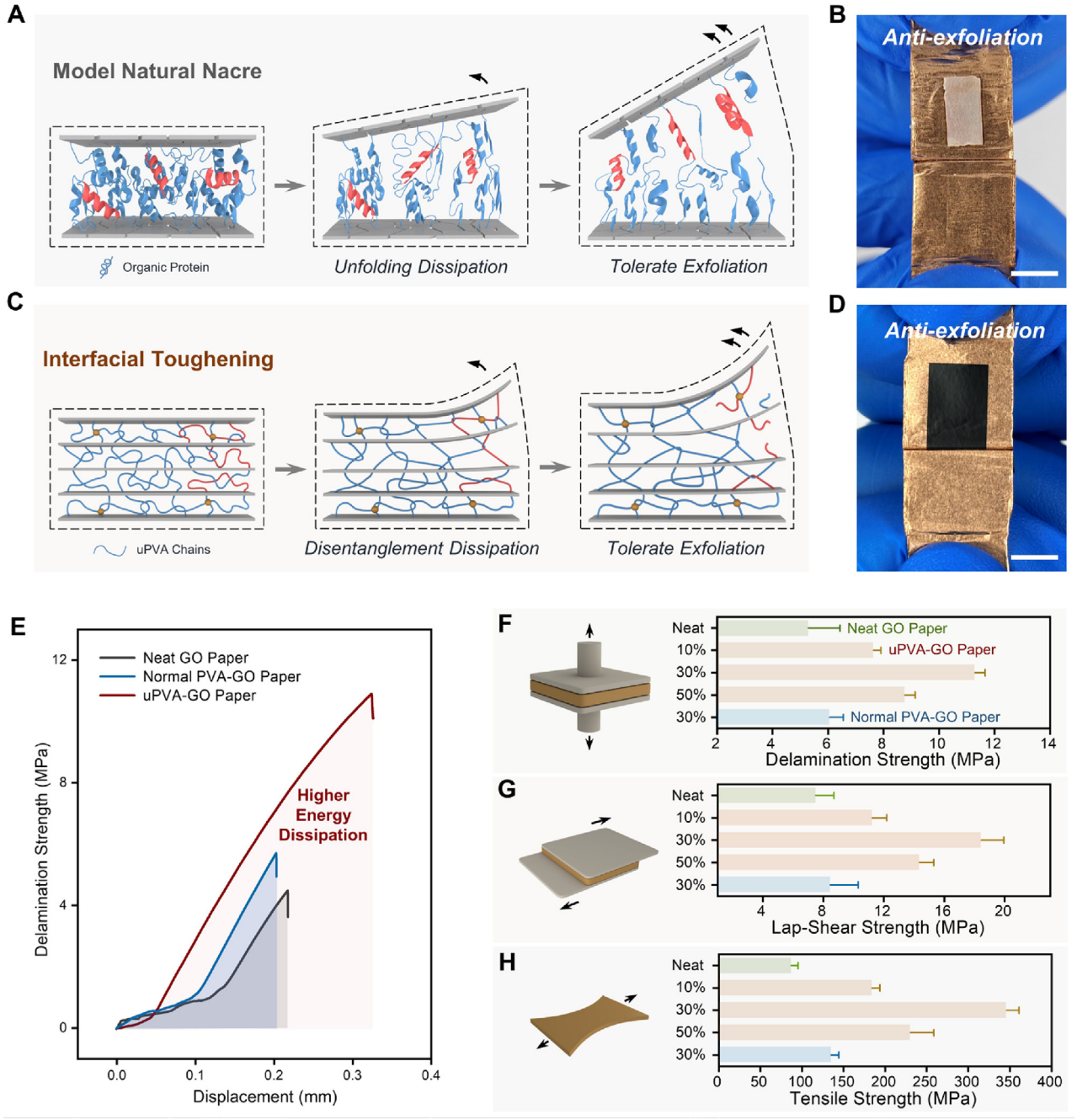

FIG. 2

Artificial interfacial entanglement toughening design and delamination behavior analysis. (**A**) Schematic of the tolerate exfoliation mechanism contributed by interlayer protein glue in natural nacres. The blue coiling lines represent organic proteins such as Lustrin A and Pif97 [33]. The red lines emphasize the unfolding process during delamination deformation. (**B**) Photograph of the tape peeling test of natural nacre, showing well anti-exfoliation performance result from no remains on the tape surface. The scale bar is 0.5 cm. (**C**) Schematic of the tolerate exfoliation mechanism contributed by disentanglement energy dissipation in our IET papers. The blue entangled lines represent uPVA chains and the yellow balls represent physical crosslinking points by intramolecular hydrogen bonds. The red lines emphasize the disentanglement process during delamination deformation. (**D**) Photograph of the tape peeling test of IET-GO papers. The scale bar is 0.5 cm. (**E**) The strength–displacement curves of three typical samples with different interlayer energy dissipation abilities. (**F**-**H**) Schematic of the delamination test and the delamination strength (F), lap-shear test and the shear strength (G), tension test and the tensile strength (H) of samples with different PVA concentrations and molecular weight.

including pulling out edges and microscale bumps in the exfoliated planes. Wrinkle analysis of the delamination failure section demonstrates that the IET-GO paper has a roughness degree of 350 nm, much higher than that (230 nm) of neat GO paper (Fig. S13).

The interlayer uPVA acts as the soft phase to enhance the plastic dissipation capability to relieve the delamination stress concentrating and resist the delamination failure (Fig. 3E-H) [40]. The closer force mapping of delamination surface revealed that uPVA forms soft bumps (height of ~180 nm and width

Please cite this article in press as: K. Li et al., Materials Today (2025), https://doi.org/10.1016/j.mattod.2025.02.011

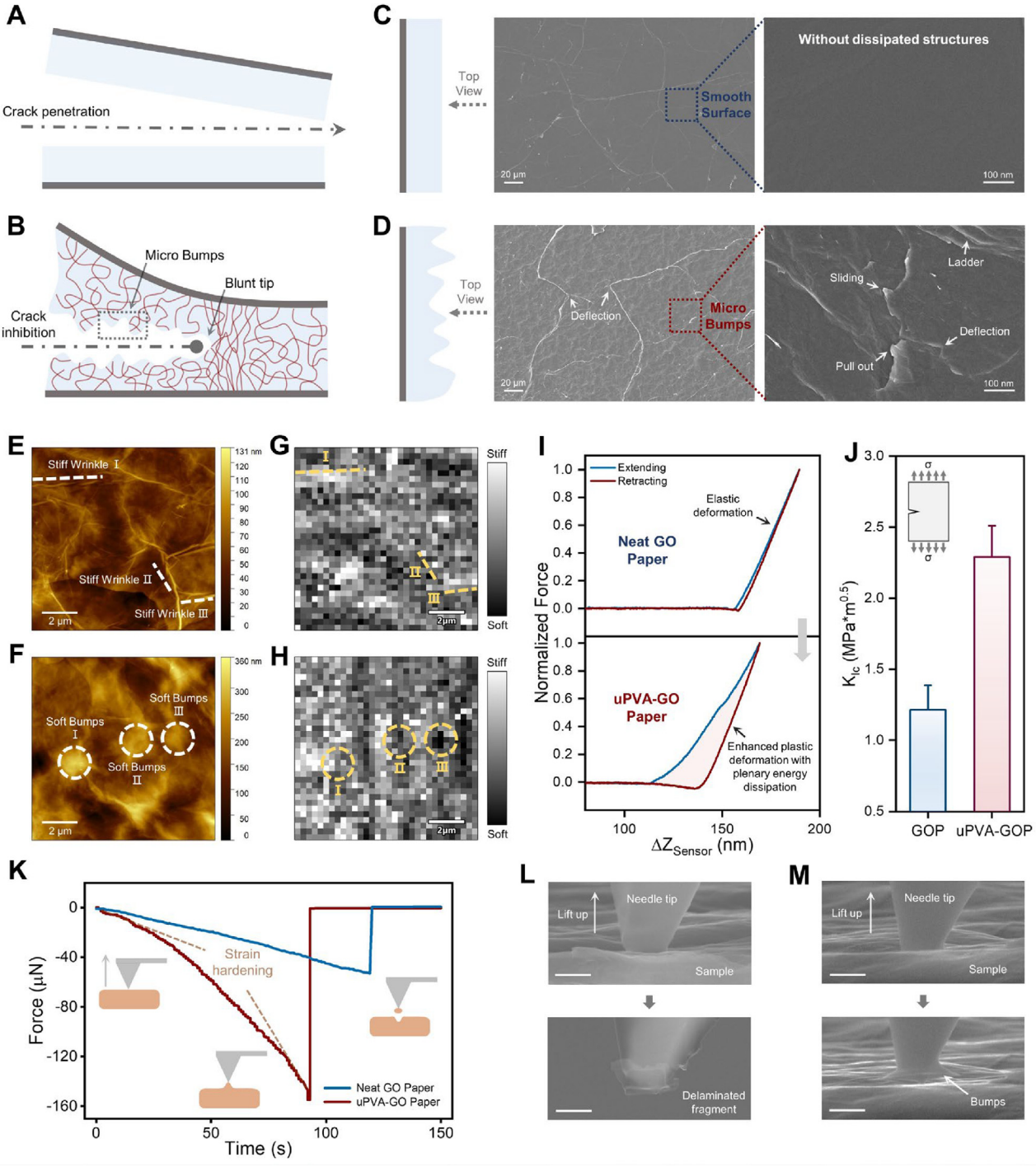

FIG. 3

Mechanism analysis of artificial interfacial entanglement toughening. (**A** and **B**) Schematic of delamination crack propagation behavior of neat GO papers (A) and uPVA-GO papers (B). (**C**-**F**) SEM images and AFM height phase images of the delamination fracture surfaces of neat GO papers (C and E) and uPVA-GO paper (D and F). (**G**, **H**) Fast force volume mappings of neat GO papers (G) and uPVA-GO papers (H), the light portion means a relatively higher force region. (**I**) AFM normalized force-ΔZ_{sensor} curve of neat GO papers and uPVA-GO papers. (**J**) Critical stress intensity factor (K_{Ic}) resulting from single-edge notched test for two kinds of papers. (**K**) In-situ adhering force curves of neat GO papers and uPVA-GO paper. The inset picture are the schematic of three stages in test process. (**L**, **M**) SEM images of the in-situ adhere probing test process of neat GO papers (L) and uPVA-GO papers (M) during the in-situ adhering test. The scale bars are 1 μm.

of ~1 μm) after delamination, enhancing the intrinsic toughness to resist exfoliation failure [50]. We tested the nanoindentation deformation response of neat GO and uPVA-GO papers [51]. Neat GO paper exhibits an elastic interlayer deformation behavior but uPVA-GO paper demonstrates a plastic deformation behavior to exhaust the interlayer stress and toughen the lamellar structure (Fig. 3I). The intrinsic toughening mechanism of IET strategy is confirmed by the higher critical stress intensity

Please cite this article in press as: K. Li et al., Materials Today (2025), https://doi.org/10.1016/j.mattod.2025.02.011

factor (K_{Ic}) of uPVA-GO paper (~2.2 MPa·$m^{0.5}$) than that (~1.2 MPa·$m^{0.5}$) of neat GO paper, measured by the standard single-edge notched test (Fig. 3J, S14) [40,52]. Beside the enhanced delamination resistance, IET strategy improved the lap-shear, tensile strength and out-of-plane bending strength of GO papers (Fig. S10, S11, S15).

We monitored the exfoliation at microscale by the in-situ adhere probing test [53]. For neat GO paper, the sticky needle can clearly peel off small debris (Fig. 3L). By contrast, the smooth surface of uPVA-GO paper deformed to bump around the lifting probe tip (Fig. 3M), evidencing the resistance against easy exfoliation as observed in peeling surface morphology (Fig. 3F, H). The record force curves demonstrate the higher energy dissipation capability to resist exfoliation (Fig. 3K). The delamination curve of uPVA-GO paper features a strain hardening trend to dissipate more energy as compared with the elastic curve of neat GO paper, resulting from the enhanced inter-chain friction by intramolecular hydrogen bonding of uPVA [18,54–57]. The ultimate exfoliation force of uPVA-GO paper (160 μN) is nearly 2-times higher than that (50 μN) of neat GO paper, revealing the efficiency of IET strategy to resist delamination failure.

Through IET method, lamellar GO materials start to have a comparable delamination strength to the benchmark natural nacre, complementing the outstanding in-plane performances with high out-of-plane failure resistance (Fig. 4). The MD simulations at the molecular scale also reveal that the highly entangled polymer chains help loading transfer between GO sheets, providing strong energy dissipation by disentanglement, slipping, and surging at high strains to prevent GO sheet edges from sliding apart in the fracture process [18,56]. In the previous trend, chemical crosslinking and van der Waals interaction can enhance the interlayer bonding and in-plane strength up to a

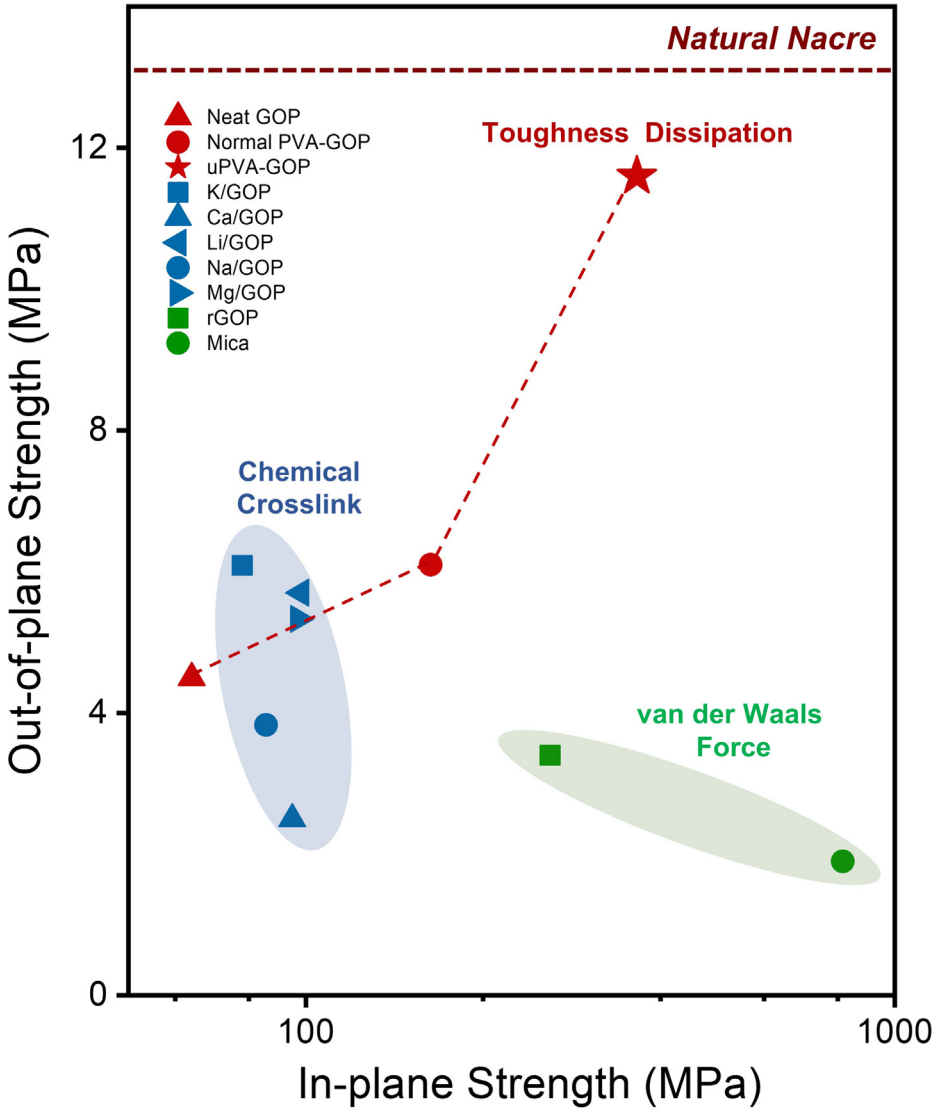

FIG. 4

Comparison in strength between in-plane direction (tensile strength) and out-of-plane direction (delamination strength) of 2D assembly materials with diverse interlayer interaction. The green region means 2D materials assembled by van der Waals force such as π-π stacking. The blue region means 2D materials assembled by chemical crosslinks such as electrovalent bonds. The red star means our artificial interfacial entanglement toughening design, showing an effective synergy enhancement of the delamination strength and tensile strength for graphene assembly materials.

Please cite this article in press as: K. Li et al., Materials Today (2025), https://doi.org/10.1016/j.mattod.2025.02.011

remarkable level of ~2 GPa [19], but gives a neglectable improvement in delamination resistance. In contrast to the greatly expected use as realistic structural materials, the increasing in-plane strength conversely brings a greatly deteriorated delamination resistance. The resulting low fracture toughness would be no means of relieving any local high stresses and where cracks once initiated, immediately propagate in an unstable and often catastrophic fashion, especially under the large out-of-plane deformation [40]. Beyond the previous trend, IET method can balance the in-plane strength merit and the outstanding delamination resistance, enabling the lamellar 2D materials usable to approach realistic applications.

Delamination resistant functional lamellar materials

Using IET strategy to relieve the delamination deficiency, we fabricated the uPVA-reduced graphene papers (IET-rGO) and their laminated composite bulks with epoxy resin (Fig. 5A). The IET-rGO bulk exhibited an excellent bending strength of 163.5 MPa, which is almost three times higher than that (~35 MPa) of the neat rGO bulks (Fig. 5D). The high bending

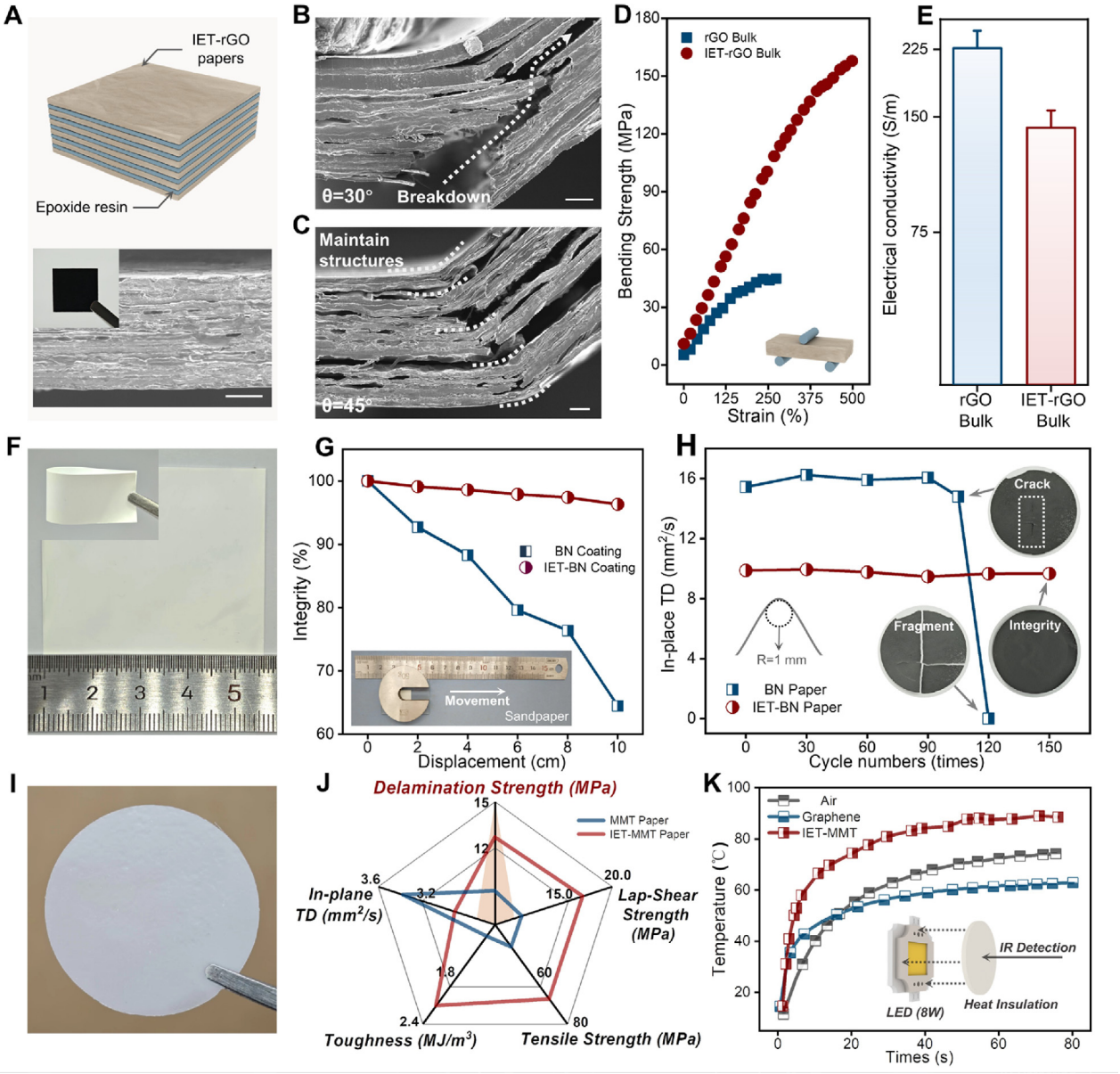

FIG. 5

Interlayer entanglement toughing 2D lamellar composites. (**A**) Schematic and photos of IET-rGO composite bulks and the SEM image of the cross-section. The scale bar is 30 μm. (**B**, **C**) SEM images of the bending failure for rGO bulks (B) and IET-rGO bulks (C). The scale bar is 20 μm. (**D**) The three-point bending strength–strain curves of rGO bulks and IET-rGO bulks. The strain is calculated by dividing the displacement of the indenter by the thickness of the sample. (**E**) Electrical conductivity of two composite bulks. (**F**) Photos of IET-BN coating on PP separator membranes. (**G**) The wear resistance curves of two kinds of coatings. Insert picture is the digital photo of the wear resistance test. The weight is 50 g and the sandpaper is 600 mesh. (**H**) The cycle bending in-plane thermal diffusivity (TD) testing of two kinds of freestanding papers. The curvature radius is 1 mm and the inserts are photos of samples (D = 25 mm). (**I**) Photo of IET-MMT papers. (**J**) Mechanical and thermal performance characterizations for two kinds of MMT papers. (**K**) Central temperature evolution versus running time of the LED matrix with different heat insulations and the schematic of the test system.

Please cite this article in press as: K. Li et al., Materials Today (2025), https://doi.org/10.1016/j.mattod.2025.02.011

strength of IET-rGO bulks results from the improved delamination resistance of IET-rGO papers, which allows the resin to bind laminated papers tightly together, enhancing the fracture toughness and inducing a mix-mode fracture of bulks which is helpful to increase the resistance of crack propagation (Fig. 5C) [58]. Otherwise, the delamination failure easily occurs at the interface between papers and resins, even at mild curvature (Fig. 5B), which is a fatal failure for the structural bulks, regardless the high in-plane strength. Meanwhile, benefitting from the relatively low containing of the ultra-high molecular weight polymer, the electrical conductivity of IET-rGO composite bulk shows a mildly degrading by 37 % as compared to the neat rGO composite bulk at the same resin containing (Fig. 5E).

Extending from the model graphene based materials, the IET strategy was also applicable for preparing delamination resisting materials of other typical 2D sheets, such as boron nitride (BN) and montmorillonite (MMT). We fabricated a durable IET-BN coating with excellent wear-resisting property, which can prevent the sliding of tablets and hold the structure integrity during violent shear and bending deformation (Fig. 5F-H, S16). This IET-BN coating kept the stable in-plane thermal diffusivity (TD) during cyclic bending with a small bending radius of 1 mm, outperforming the abrupt fragmentation of neat BN coating (Fig. 5H, S16). We fabricated freestanding IET-MMT paper by vacuum filtration (Fig. 5I). The strong entanglement of uPVA effectively toughened the MMT interlayer interaction and greatly improved the overall mechanical performances in both in-plane and out-of-plane directions (Fig. 5J). The delamination failure section of IET-MMT paper exhibited typical dissipation structures, resembling the same strengthen mechanism of IET-GO (Fig. S17). The low TD with high delamination resistance of IET-MMT paper can find realistic applications in the thermal insulation (Fig. 5K, S18).

Discussion

2D sheet and their assembled materials have ignited great expectations for the past two decades [59,60]. Numerous researches have demonstrated the outstanding in-plane performances of their prototype assembled materials, which is the spirit of utilizing the planar properties of 2D sheets [10,61]. Beyond these dominating merits, any fatal deficiency would disable the prevailing uses to meet the all-round requirements of realistic applications, which should be paid more researching attentions [62]. In this paper, we caught a paradox of delamination behind the outstanding in-plane performances of 2D sheet assembled materials, which could become the hidden fatal deficiency to hinder their realistic applications.

By comparative analysis, a contradictive trend was unveiled as the enhancing packing order of 2D sheets of their neat laminated materials generates an aggravating delamination failure (Fig. 1D). This counterintuitive trend denotes that the prevailing enhancement stacking order or interlayer binding strength is hard to meet the complex deformation in realistic applications. The dominating mechanism of resisting delamination is the interlayer dissipation, but not the mere stacking order and interlayer binding, which is the mechanism of nature nacre to keep structural integration and resist delamination by interlayer proteins [33].

Inspired by the natural nacre, we proposed a strategy to resolve the long-ignored delamination weakness of assembled 2D materials. We introduced ultrahigh molecular weight polymer with strong chain entanglement to provide efficient interlayer energy dissipation with a low filler loading. In the IET strategy, strong interlayer entanglement enriches the energy dissipation pathway and alleviates the stress concentration of the crack slits and suppress delamination propagation, achieving desirable balance between the intrinsic conflicted in-plane and out-of-plane strength. The GO model materials exhibited comparable resistance strength of benchmark nature nacres.

The IET strategy can extend to the general assembled materials of 2D sheets. A series of delamination resisting materials with favorable functions were verified extending from reduced graphene to BN and MMT. The IET strategy acts as efficient method to relieve the ignored delamination failure and points a pathway to balance the all-round properties of 2D sheets assembled materials for wide realistic applications, ranging from structural components to coating and functional materials.

Experimental procedures

Resource availability

Lead contact

Further information and requests for resources and reagents should be directed to and will be fulfilled by the Lead Contact, Zhen Xu (zhenxu@zju.edu.cn).

Materials availability

This study did not generate new unique reagents.

Data and code availability

All the necessary data to evaluate the main conclusions of this paper have been presented in the main text and Supplemental Information. Additional data related to the paper can be obtained from the authors upon request.

Fabrication of GO and IET-GO papers

GO aqueous dispersions were purchased from Hangzhou Gaoxi Technology Co., Ltd. (Fig. S19). Sodium MMT powders were purchased from Zhejiang Fenghong New Material Co., LTD. PVA powders were purchased from energy chemical. IET-GO papers with different PVA mass fractions were prepared by mixing the given amount of GO (5.7 mg/ml) and PVA (5 wt%) dispersions. Uniform dispersion was cast-dried on the PET substrate at 25°C for 48 h and peeled off to obtain freestanding neat GO, normal PVA GO and IET-GO papers (Fig. S20).

Fabrication of metal crosslinked GO papers

As-prepared GO papers were immersed in 0.25 M NaCl, KCl, LiCl, $CaCl_2$ and $Mg(CH_3COO)_2$ solution at room temperature for 2 h respectively [63]. Then the crosslinked papers were washed by DI water three times to remove residual salt ions on the surfaces and dried at 25°C for 12 h.

Please cite this article in press as: K. Li et al., Materials Today (2025), https://doi.org/10.1016/j.mattod.2025.02.011

Fabrication of IET-rGO/Resin composites

As-prepared IET-GO papers (30 wt% uPVA) were fixed both sides on the glass plate and reduced by the mixture of HI and acetic acid (1:3 v/v) at 90°C for 24 h. Residual HI was removed by heating at 105°C for 12 h under vacuum. Reduced IET-GO papers (IET-rGO papers) were cut to 1 x 1 cm with 30 pieces by mold and bonded with epoxy resin (purchased from Wells Advanced Materials (Shanghai) Co., Ltd) by heating under pressure.

Fabrication of IET-BN coatings

A dispersion of BN flakes in DI water was prepared using a PSI-20 high pressure homogenizer. The dispersion, consisting of 400 mL of DI water, used 100 g/L of boron nitride flakes as the starting material. Sodium deoxycholate (SDC) at a concentration of 9 g/L served as the surfactant, and carboxymethylcellulose sodium salt (CMC) at 10 g/L was added as a rheology modifier. The mixture was processed through 50 cycles in the homogenizer, with each cycle involving a complete pass of the 400 mL mixture through the interaction chamber of the homogenizer. IET-BN dispersions (30 wt% PVA) were prepared by mixing the given amount of BN (2 wt%) and PVA (5 wt%) dispersions. Plasma cleaned commercial polyolefin separator (Celgard (PP) separator) was placed on a flat surface and IET-BN dispersions was then spread on it by Mayer-bar. Coated separator was dried at 45°C for 24 h. IET-BN papers were prepared by casting IET-BN dispersions (30 wt% PVA) on substrate and dried at 25°C for 48 h.

Fabrication of IET-MMT papers

Dispersion of MMT in deionized water (1 wt%) was stirred thoroughly for 10 days and then centrifuged at 3000 rpm for 15 min twice to remove unexfoliated MMT. IET-MMT papers were fabricated by vacuum filtering with the obtained dispersion on the cellulose acetate filtration paper (pore size of 0.2 mm) and then dissolving the filtration paper in acetone.

Delamination strength measurement

In the delamination test, paper samples were cut to a circle plate with diameter of 5 mm by mold, and adhered to a glass slide by epoxy resin (3 M DP420). Nacre samples were fabricated by manual sandpaper burnishing. Then, we attached an as-burnished extrusion-rivet bolt with diameter of 4.6 mm to another sild of the sample on glass by epoxy resin. Before the test, we adhered the glass to a T-shaped machined part by quick-drying adhesive and used a plate machined part with thread for easily clamping. And we used a hexagonal nut to relieve the assembly stress and keep the loading direction is vertical to sample surface (Fig. S21). All samples were run in decuple. Additional information related to the test can be obtained from the Supplemental Information.

In-situ adhere probing test

In the in-situ adhere probing test, the force sensor was calibrated by a spring with a standard stiffness of 9.38 μN/μm. After calibration, the atomic force microscope (AFM) tip was moved to the silicon substrate under low voltage and dipped the SEM glue on the tip. Then the tip was moved to the sample and adhered to the sample surface by raising the electron beam intensity and curing the glue. After completely curing, the tip was lifted with a uniform velocity and the change of force value could be recorded.

Characterizations

The mechanical tests were carried on different electronic universal testing machines. The Instron 5943 was used for out-of-plane drawing and lap-shear test at a loading rate of 0.3 mm/min. The Instron 2344 was used for tension test at a loading rate of 2 mm/min and the gauge length was 5 mm. The Reger RGWT-4000–20 was used for single-edge notched test and three-point bending test at a loading rate of 0.06 and 1 mm/min respectively.

The structure and surface morphology were investigated by optical microscopy (Nikon E600POL), optical profilometer (Wyko NT9100), XRD (X'PertPro PANalytical diffractometer), SEM (Carl-Zeiss EVO-10, sigma 500 and Hitachi S4800) and AFM (Cypher ES). The electrical conductivity was measured by two-probe method on the Keithley 2400 multiple-function source-meter. The thermal performance were measured by laser scattering equipment (LFA 467, Netzsch, Germany) and thermal infrared imager (T630sc, FLIR, USA).

CRediT authorship contribution statement

Kaiwen Li: Writing – review & editing, Writing – original draft, Visualization, Validation, Methodology, Investigation, Formal analysis, Data curation, Conceptualization. **Lidan Wang:** Methodology, Investigation, Data curation. **Feifan Chen:** Formal analysis, Data curation. **Jiahao Lu:** Formal analysis, Data curation. **Rui Guo:** Formal analysis, Data curation. **Yue Gao:** Formal analysis, Data curation. **Shiyu Luo:** Data curation. **Xin Ming:** Supervision, Formal analysis. **Yue Lin:** Formal analysis, Data curation. **Zhen Xu:** Writing – review & editing, Supervision, Resources, Project administration, Funding acquisition, Conceptualization. **Manyi Huang:** Data curation. **Chao Wang:** Writing – review & editing, Supervision, Resources, Funding acquisition, Conceptualization. **Yingjun Liu:** Writing – review & editing, Supervision, Funding acquisition, Conceptualization. **Chao Gao:** Writing – review & editing, Supervision, Resources, Funding acquisition, Conceptualization.

Data availability

No data was used for the research described in the article.

Declaration of competing interest

The authors declare that they have no known competing financial interests or personal relationships that could have appeared to influence the work reported in this paper.

Acknowledgments

We thank Yujie Zhao from Department of Polymer Science and Engineering, Zhejiang University and Xinning Zhang from Testing and Analysis Center of Department of Polymer Science and Engineering, Zhejiang University for the assistance in performing atomic force microscopy (AFM) measurements.

Funding

This work is financially supported by the funding as listed below:

National Natural Science Foundation of China (nos. 52,122,301 to Z.X., 52,090,030 to C.G., 12,372,108 to C.W. and 52,272,046 to Y.J.L.).

National Key Research and Development Program of China (2022YFA1205300 to Z.X. and 2022YFA1205301 to Z.X.).

"Pioneer" and "Leading Goose" R&D Program of Zhejiang (2023C01190 to Z.X.).

The Fundamental Research Funds for the Central Universities (nos. 226–2024-00074 to Z.X. and 226–2023-00023 to Y.J.L.).

Author contributions

Z.X., C.W., Y.J.L. and C.G. conceived the research. K.W.L. designed experiments, analyzed the data, and wrote the manuscript. K.W.L., L.D.W., F.F.C. and R.G. did the mechanical test of samples. K.W.L., J.H.L. and S.Y.L. did the electrical and thermal test of samples. K.W.L., Y.G. and X.M. did the fundamental characterization of GO sheets. Y.L. fabricated the BN dispersion. M.Y.H. did the in-situ adhere probing test of samples.

Data and materials availability

All data needed to evaluate the conclusions in the paper are present in the paper and/or the Supplementary Materials.

Appendix A. Supplementary material

Supplementary data to this article can be found online at https://doi.org/10.1016/j.mattod.2025.02.011.

References

[1] K.S. Novoselov et al., *Science* 306 (5696) (2004) 666.
[2] C.J. Castilho et al., *Carbon* 173 (2021) 410.
[3] H. Li et al., *Small* 9 (11) (2013) 1974.
[4] A.P. Rooney et al., *Nat. Commun.* 9 (1) (2018) 3597.
[5] J.Y. Moon et al., Sci. Adv. 6 (44) (2020) eabc6601.
[6] A. Islam et al., *ACS Nano* 15 (1) (2021) 1775.
[7] H.L. Wang et al., *Small* 17 (34) (2021) 2102263.
[8] Q.W. Yan et al., *ACS Nano* 15 (4) (2021) 6489.
[9] M. Naguib et al., *Adv. Mater* 23 (37) (2011) 4248.
[10] P. Li et al., *Nat. Commun.* 11 (1) (2020) 2645.
[11] M. Zhang et al., *Adv. Mater.* 27 (42) (2015) 6708.
[12] P. Li et al., *Nat. Commun.* 15 (1) (2024) 409.
[13] W. Eom et al., *Nat. Commun.* 11 (1) (2020) 2825.
[14] X. Ming et al., *Adv. Mater.* 34 (2022) 28.
[15] W.T. Gan et al., *Adv. Funct. Mater.* 30 (10) (2020) 1909196.
[16] T.Z. Guo et al., *Adv. Funct. Mater.* 33 (15) (2023) 2213183.
[17] S. Wan et al., *Nat. Mater.* 20 (5) (2021) 624.
[18] L. Wang et al., *Nano Lett.* 23 (8) (2023) 3352.
[19] J. Yang et al., *Science* 383 (6684) (2024) 771.
[20] W. Li et al., *Science* 385 (6704) (2024) 62.
[21] W. Wang et al., *Nat. Commun.* 6 (2015) 7853.
[22] H. Sakuma, S. Suehara, *J Geophys Res-Sol Ea* 120 (4) (2015) 2212.
[23] M. Daly et al., *ACS Nano* 10 (2) (2016) 1939.
[24] F. Najafi et al., *Compos. Sci. Technol.* 194 (2020) 108140.
[25] S.J. Wan et al., *Adv. Mater.* 28 (36) (2016) 7862.
[26] Y.W. Quan et al., *Carbon* 226 (2024) 119179.
[27] J.Y. Zhu et al., *Nat. Mater.* 23 (5) (2024) 604.
[28] W.H. Xie et al., *Carbon* 213 (2023) 118268.
[29] W.H. Xie, Y.J. Wei, *Nano Lett.* 21 (11) (2021) 4823.
[30] S.M. Chen et al., *Sci. Adv.* 10 (2024) 14.
[31] A. Hassan et al., *ACS Appl. Mater. Interfaces* 13 (49) (2021) 59478.
[32] E.Y. Jeon et al., *Biomaterials* 222 (2019) 119439.
[33] F. Barthelat et al., *Nat. Rev. Mater.* 1 (4) (2016) 16007.
[34] A.P. Jackson et al., *Proc R Soc Ser B-Bio* 234 (1277) (1988) 415.
[35] B.L. Smith et al., *Nature* 399 (6738) (1999) 761.
[36] T. Cui et al., *Carbon* 136 (2018) 168.
[37] C.X. Zhang et al., *Carbon* 171 (2021) 417.
[38] J. Zhong et al., *Nat. Commun.* 9 (1) (2018) 3484.
[39] P. Zhang et al., *Nat. Commun.* 5 (2014) 3782.
[40] R.O. Ritchie, *Nat. Mater.* 10 (11) (2011) 817.
[41] X. Wang et al., *Nat. Commun.* 11 (1) (2020) 211.
[42] S. Wan et al., *Adv. Mater.* (2018) e1802733.
[43] J.Y. Woo et al., *ACS Nano* 13 (4) (2019) 4522.
[44] J. Kim et al., *Science* 374 (6564) (2021) 212.
[45] L. Mao et al., *Nat. Commun.* (2019) 10.
[46] G.J. Liang et al., *Npj Flex Electron* 5 (1) (2021) 27.
[47] D.M. Tang et al., *Nat. Commun.* 5 (2014) 3631.
[48] B. Xue et al., *Nat. Commun.* 12 (1) (2021) 7156.
[49] R. Rabiei et al., *Acta Biomater.* 6 (10) (2010) 4081.
[50] A.H. E et al., *Biophys. J* . 74 (3) (1998) 1564.
[51] J.P. Aime et al., *J. Appl. Phys.* 76 (2) (1994) 754.
[52] Y. Jiang et al., *Mater. Horiz.* 10 (2) (2023) 556.
[53] G. Cheng et al., *Small* 20 (34) (2024) e2401635.
[54] Y.Z. Hou et al., *ACS Nano* 15 (1) (2021) 1310.
[55] S.C. Zhang et al., *Adv. Mater.* 36 (2024) 35.
[56] L.D. Wang et al., *Nano Lett.* 24 (14) (2024) 4256.
[57] M.A. Rahman et al., *Sci. Adv.* 7 (2021) 42.
[58] X.G. Zeng, Y.J. Wei, *J. Mech. Phys. Solids* 101 (2017) 235.
[59] J. Lipton et al., *Matter-Us* 2 (5) (2020) 1148.
[60] F. Wang et al., *Appl. Phys. Rev.* 10 (1) (2023) 011311.
[61] P. Li et al., *Adv. Funct. Mater.* 30 (52) (2020) 2006584.
[62] M. Zeng et al., *Chem. Rev.* 118 (13) (2018) 6236.
[63] L. Chen et al., *Nature* 550 (7676) (2017) 380.

Please cite this article in press as: K. Li et al., Materials Today (2025), https://doi.org/10.1016/j.mattod.2025.02.011